Nanostructured Magnetic Thin Films from Organometallic Block Copolymers: Pyrolysis of Self-Assembled Polystyrene-*block*-poly(ferrocenylethylmethylsilane)

David A. Rider,[†] Kun Liu,[†] Jean-Charles Eloi,[‡] Lawrence Vanderark,[†] Ling Yang,[§] Jia-Yu Wang,[§] Dan Grozea,[⊥] Zheng-Hong Lu,[⊥] Thomas P. Russell,[§,*] and Ian Manners[‡,*]

[†]Department of Chemistry, University of Toronto, Toronto M5S 3H6, Canada, [‡]School of Chemistry, University of Bristol, Bristol BS8 1TS, United Kingdom, [§]Department of Polymer Science and Engineering, University of Massachusetts, Amherst, Massachusetts 01003, and [⊥]Department of Materials Science and Engineering, University of Toronto, Toronto M5S 3E4, Canada

ABSTRACT The pyrolysis of cylinder-forming samples of the diblock copolymer polystyrene-*block*-poly(ferrocenylethylmethylsilane) (PS-*b*-PFEMS) in bulk and in thin films has confirmed that these materials are useful for the generation of semi-ordered arrays of C/SiC ceramics containing Fe nanoparticles which are derived from the organometallic domains. In many cases, the ceramic mass yields were predictable and produced ceramics bearing a monomodal distribution of iron nanoparticles due to the nanoscaled structure of the preceramic PFEMS domains. The pyrolysis of thin films stabilized by cross-linking the PS domains with UV light demonstrated high areal yields, improved shape retention, and the presence of cylinder-centered magnetic nanoparticles.

KEYWORDS: self-assembly · nanomaterials · magnetic particles · nanotechnology · polyferrocenylsilane · block copolymer lithography · nanostructured ceramic

The ability to produce well-ordered arrays of well-defined and periodic nanostructures is critical to the advancement of high feature density technologies such as magnetic data storage and microelectronics.[1–3] Serial procedures, often executed by top-down techniques, are currently the dominant methods of choice in these areas. The converse bottom-up approach, where parallel access to nanostructures is much more cost-effective and rapid, can outperform many top-down patterning techniques in terms of feature size, periodic length scale, and simplicity.[4–8] Block copolymer lithography represents a very promising tool in these respects due to many recent breakthroughs.[9–16] To date, the role of the block copolymer material has been sacrificial in most cases. Typically, self-assembled block copolymers are used to construct a template (by way of either solution-state structures capable of loading or thin films capable of site-specific modifications, or combinations thereof) that is ultimately used for negative or positive patterning of a material of interest. The use of functional block copolymers for nanolithography, where the polymer directly creates the desired nanostructured material, is rare.[17–19]

Diblock copolymers, macromolecules comprised of two different polymer segments covalently linked at a common junction, spontaneously self-assemble into well-ordered arrays of nanometer-sized microdomains.[4,20] Morphologies ranging from spherical to cylindrical, gyroid, or lamellar are accessible, depending on the volume fraction of the components, φ, while the molecular weight (M_n) dictates the domain size.[21] Additional interest and opportunities arise when one of the polymer blocks is rich in transition metal centers. Metal-containing block copolymers thus exhibit novel characteristics due to the presence of the redox-active, photophysical, conductive, catalytic, or preceramic metalloblock.[22,23] Polyferrocenylsilanes (PFS), a well-studied class of organometallic polymers with iron atoms in the main chain, are readily available *via* the ring-opening polymerization (ROP) of ring-strained sila[1]ferrocenophane monomers.[24–28] Additionally, PFS block copolymers can be synthesized by sequential living anionic polymerization.[29,30] In the solid state, PFS block copolymers undergo microphase separation into iron-rich nanodomains[31–38] and have attracted

*Address correspondence to Russell@mail.pse.umass.edu, Ian.Manners@bristol.ac.uk.

Received for review September 28, 2007 and accepted January 09, 2008.

Published online February 26, 2008.
10.1021/nn7002629 CCC: $40.75

recent attention due to their redox-induced morphology changes and their functions as precursors to magnetic or catalytic materials and as plasma etch-resistant nanotemplates.[12,19,39–42] The focus of this study was to investigate the ability of cylinder-forming polystyrene-*block*-poly(ferrocenylethylmethylsilane) (PS-*b*-PFEMS) to act as a functional block copolymer capable of both templating and producing nanostructured ceramics from its constituent elements.[19] Rather than conventional reactive ion etch processing, our approach makes use of a simple pyrolysis procedure capable of reducing ferrocenyl units to their metallic elemental state as well as generating a stable and inert SiC/C matrix from the preceramic polymer.[43–46] In this paper we report that, for PS-*b*-PFEMS films: (i) the PFEMS nanodomains formed by block copolymer self-assembly function as efficient ceramic precursors; (ii) the PS segments, which are glassy at room temperature, can be easily cross-linked and therefore stabilize thin films during subsequent pyrolysis; and (iii) nanostructured magnetic ceramic arrays are easily afforded when (i) and (ii) are executed.

RESULTS AND DISCUSSION

The diblock copolymers used for pyrolysis studies were PS-*b*-PFEMS(0.25) and PS-*b*-PFEMS(0.36), where the fraction in parentheses denotes the volume ratio of PFEMS (φ_{PFEMS}). The former is composed of a PS segment with M_n = 27 400 g/mol and a PFEMS segment with M_n = 11 300 g/mol, whereas the latter contains an M_n = 40 500 g/mol PS segment and an M_n = 27 700 g/mol PFEMS segment. The respective polydispersity indices were 1.01 and 1.04, as determined by gel permeation chromatography (GPC) using a triple detector. Both materials afforded cylindrical morphologies in the bulk.[37,47] To provide insight into ceramic yields from thermogravimetric analysis (TGA), we used two additional homopolymers, namely PS and PFEMS.[37] The molecular characteristics and morphological dimensions of the homopolymers and diblock copolymers are summarized in Table 1. A schematic representation of our pyrolysis investigations of bulk and thin film samples of cylinder-forming PS-*b*-PFEMS block copolymers is depicted in Scheme 1.

TABLE 1. Molecular Characteristics and Morphological Dimensions of the Homopolymers and Diblock Copolymers Used in This Study

polymer	M_n (PDI)[a]	φ_{PFEMS}	$D_{c\text{-}c}$ (nm)[b]	d_{cyl} (nm)[c]
PS	29 300 (1.02)	0		
PFEMS	10 000 (1.01)	1		
PS-*b*-PFEMS(0.25), bulk	38 700 (1.01)	0.25	27.9	15.7
PS-*b*-PFEMS(0.36), bulk	68 200 (1.04)	0.36	42.5	28.7

[a]For block copolymers, from GPC of PS aliquot sampled during synthesis and ^{1}H NMR data. By GPC, the standard deviations for M_n and PDI were estimated to be ~5% and ~1%, respectively. [b]Bulk periodicity, $D_{c\text{-}c} = 4\pi/(\sqrt{3}q^*)$, where q^* is the primary scattering peak as determined by small-angle X-ray scattering. [c]Bulk cylinder diameter, $d_{cyl} = 2\sqrt{(D_{c\text{-}c}{}^2\varphi_{PFEMS}/\pi)}$; where the volume prism defined by three cylinders contains half a cylinder in its volume.[37,47]

Bulk samples of PS, PFEMS, PS-*b*-PFEMS(0.25), and PS-*b*-PFEMS(0.36) were prepared and annealed as described previously.[37,47] A bulk sample of PS-*b*-PFEMS(0.25) was used for inert atmosphere (N_2 blanket) TGA, and the results were compared with those for the respective homopolymers to elucidate the pyrolysis mechanism of cylinder-forming PS-*b*-PFEMS (see Figure 1). A heating rate of 1 °C/min was used to pyrolyze to final temperature of 600 °C. The theoretical weight loss profile constructed from the PS and PFEMS TGA plots and according to the mass composition of PS-*b*-PFEMS(0.25) agreed well with the experimental TGA found for the block copolymer. On the basis of this finding, we conclude that, when cylinder-forming PS-*b*-PFEMS block copolymers are pyrolyzed, a rapid decomposition of the PS matrix occurs between 325 and 400 °C. This is supported by the complete loss of the bulk PS homopolymer sample. During this process, a partial mass loss of the PFEMS nanodomains in cylinder-forming PS-*b*-PFEMS block copolymers also occurs. This corresponds to the weight loss established for bulk PFEMS homopolymer. At ~400 °C, the organometallic domains would be expected to transform into a collection of isolated inorganic ceramic objects surrounded by a void generated from the decomposition of the organic block. Based on homopolymer studies, between ~400 and 600 °C, the cylindrical ceramics should be composed of an amorphous cross-linked SiC/C matrix with Fe nanoparticles (NPs) embedded or partially embedded within.[48] Experimentally, a slight increase in mass above 400 °C was found for the nanostructured ceramic, and we proposed that surface oxidation of exposed Fe NPs readily occurs in this

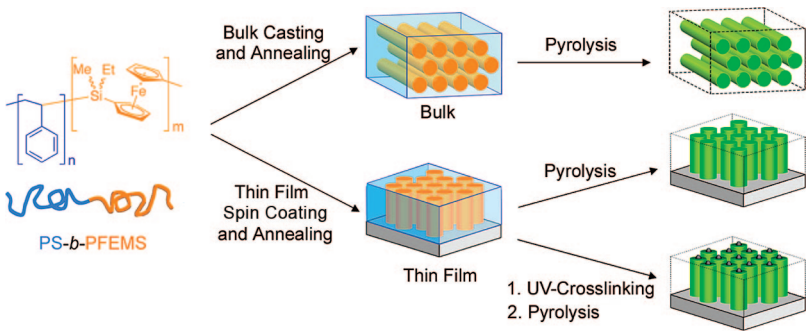

Scheme 1. Generation of ceramic materials from the pyrolysis of bulk samples (top) and thin films (below) of PS-*b*-PFEMS. For the latter, UV cross-linking is investigated for the stabilization of the thin films during the pyrolysis procedure.

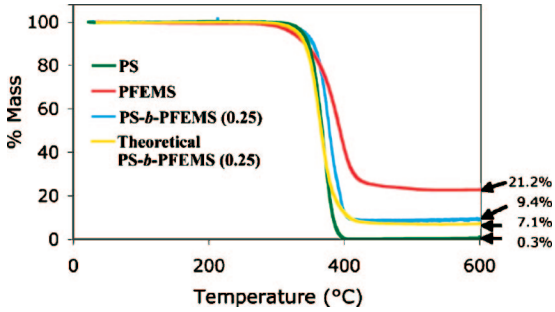

Figure 1. Thermogravimetric analysis of PS, PFEMS, and PS-*b*-PFEMS(0.25).

case due to the very high surface area established by the block copolymer lattice.[49] With further heating at 600 °C (up to 5 h), negligible mass change (<1%) was observed for all samples. We therefore conclude that PS-*b*-PFEMS block copolymers are efficient ceramic precursors that exhibit predictable ceramic yields.

A dark field transmission electron microscopy (DF-TEM) image of the bulk morphology of PS-*b*-PFEMS(0.36) is shown in Figure 2A. The cylinder diameter (d_{cyl}) and periodicity ($D_{c\text{-}c}$) for bulk PS-*b*-PFEMS(0.36) were 28.7 and 42.5 nm, respectively. This sample was divided and pyrolyzed at 600 °C in a tube furnace under an atmosphere of N_2 at a high (15 °C/min) or low (1 °C/min) heating rate. Shown in Figure 3A,B are the respective scanning electron microscopy (SEM) images of the resulting ceramics. The sample pyrolyzed at 15 °C/min produced larger, faceted iron nanoparticles which are mostly located around the cylindrical domains in the ceramic array (see Figure 3A). Based on the pyrolysis of PFS homopolymers, the composition of the array is an amorphous SiC/C matrix which houses the Fe NPs (see depiction in Figure 3C).[45,48] The average diameter of Fe nanoparticles was estimated at 48.5 nm (see Table 2), while the values for d_{cyl} and $D_{c\text{-}c}$ for the ceramic array were found to be 27.1 and 40.2 nm, respectively. When bulk cylinder-forming PS-*b*-PFEMS was pyrolyzed at lower heating rates, as in the sample depicted in Figure 3B, a collection of nanometer-scaled cylindrical ceramics was found with no large Fe nanoparticles detected by SEM. The values for d_{cyl} and $D_{c\text{-}c}$ for this ceramic lattice were 22.0 and 41.0 nm, respectively. Presumably, only small Fe NPs, <1 nm,[41,50,51] housed within the cylindrical domains of the ceramic are present in this case and are hence not easily detected by SEM.[48] This is contrary to the aforementioned ceramic array which bore many surface-located nanoparticles. The differences in the size and the location of Fe nanoparticles as a function of the heating rate suggest that higher heating rates favor decomposition and the loss of small, volatile organic fragments from PFEMS domains, which henceforth results in the formation of larger nanoparticles. The lower heating rate favors cross-linking in the PFEMS domains and leads to a slower diffusion of free Fe atoms released from PFEMS, and thus yields smaller nanoparticles. Given that the periodicity for both lattices of nanostructured ceramics is similar to that observed in bulk and that the cylinder diameters have decreased with pyrolysis, we further confirm our proposed mechanism for the pyrolysis of cylinder-forming PS-*b*-PFEMS block copolymers. It is also important to note that, in spite of heating above the order–disorder transition (ODT) temperature of the block copolymer,[33] well-defined cylindrical domains persist in the resulting ceramic materials. The high glass transition temperature (T_g) of the PS matrix is probably critical to the preservation of well-defined cylindrical domains of the low-T_g PFEMS phase in the early stages of the pyrolysis.

For thin-film pyrolysis, well-ordered, self-assembled samples of PS-*b*-PFEMS(0.25) were obtained by solvent-annealing block copolymer-coated Si wafers (see Figure 2C).[52,53] The film thicknesses were ~20 nm in all cases. A representative scanning force microscopy (SFM) image of a PS-*b*-PFEMS(0.25) film is shown in Figure 2C. In this case, d_{cyl} and $D_{c\text{-}c}$ were 14 and 28 nm, respectively. These dimensions agree with those of the bulk.[37,47] Using this as a starting material, two pyrolytic pathways were further investigated. A portion of the silicon-supported thin film of PS-*b*-PFEMS(0.25) was pyrolyzed at 1 °C/min to 600 °C. Shown in Figure 3D is the SFM height image of the resulting ceramic film. It should be noted that approximately half of the sample area is represented by these data. Remaining areas were essentially featureless, suggesting that significant disordering effects occur over half of the block copolymer thin film. It seems, therefore, that the suppression of disordering effects observed for the PS-*b*-PFEMS bulk samples is not sufficient in the pyrolysis of their thin films. Nevertheless, the inheritance of a hexagonal lattice and the inversion of contrast from Figure 2C to

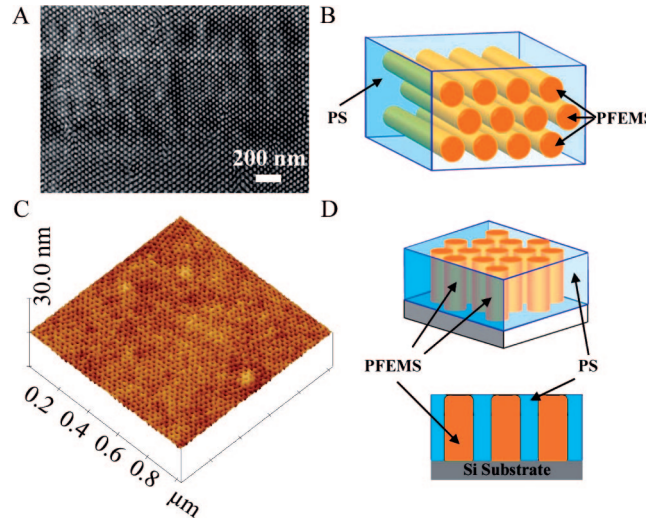

Figure 2. (A) DF-TEM image of bulk PS-*b*-PFEMS(0.36) and (B) a depiction of its bulk block copolymer structure. (C) Height-mode scanning force microscope image of annealed PS-*b*-PFEMS(0.25) thin film and (D) a depiction of its thin film structure.

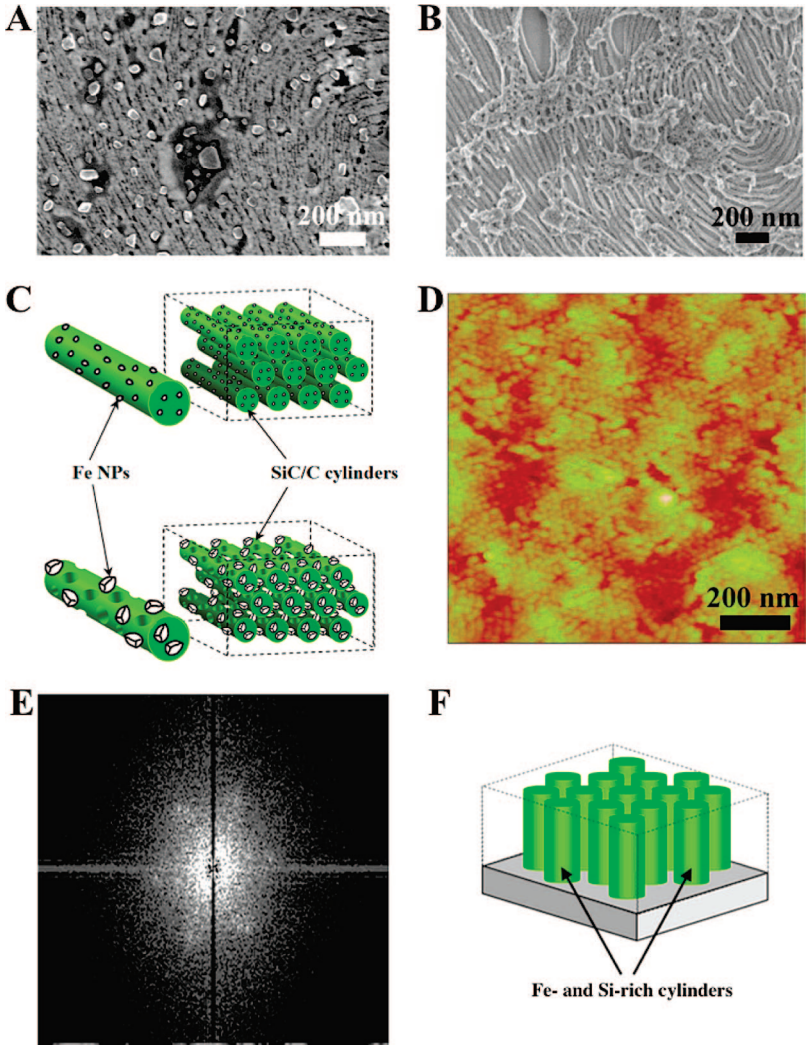

Figure 3. SEM images of the nanostructured ceramics resulting from the pyrolysis of bulk PS-*b*-PFEMS(0.36) (A) at 15 °C/min to 600 °C and (B) at 1 °C/min to 600 °C. (C) Depiction of the nanostructured ceramics in panel A at the bottom and panel B at the top. Height-mode scanning force microscope image (height scale = 10 nm) of a pyrolyzed PS-*b*-PFEMS(0.25) thin film (D) and (E) its 2D Fourier transform. (F) Depiction of the nanostructured ceramics in panel D.

some of the areas for the resulting film suggest the formation of periodic nanometer-scaled ceramics by way of (a) the volatilization of the PS matrix phase and (b) the conversion of the PFEMS domains into cylindrical iron- and silicon-rich ceramics (see Figure 3F). Shown in Figure 3E is the 2D Fourier transform of the SFM height image for pyrolyzed PS-*b*-PFEMS(0.25), which supports the formation of a hexagonal lattice and can also estimate the periodicity of the array of nanostructured ceramics. The periodicity was found to be 26 nm, a value that matches very well with its precursor film. As per our results for the bulk pyrolysis of PS-*b*-PFEMS(0.36), we assume an iron nanoparticle size of <1 nm. We attempted to investigate the magnetic properties of this sample using magnetic force microscopy (MFM). Unfortunately, no significant magnetism was detected.

It is known that PS films can be UV cross-linked.[54] To improve the shape retention in the ceramic arrays, we therefore investigated the stabilization of the self-assembled PS-*b*-PFEMS(0.25) film by way of cross-linking the organic block. For cross-linking of the PS matrix, a piece of the sample shown in Figure 2C was exposed to UV light under vacuum. Significant PS cross-linking was confirmed with a sacrificial sample by means of the insolubility of the material in various good solvents for the block copolymer (toluene, THF, dichloromethane). The pyrolysis of the sample shown in Figure 2C after UV cross-linking was then conducted under the same conditions mentioned previously (1 °C/min to 600 °C). Shown in Figure 4A−C are height-mode SFM, phase-mode MFM, and SEM images of the pyrolyzed film, respectively. In this case, the structures depicted in Figure 4 were found across the entire film area. UV cross-linking of the PS matrix is therefore a highly effective technique for increasing the areal yield of ceramic features. Previous studies on the pyrolysis of cylindrical PI-*b*-PFS (PI = polyisoprene) block copolymer micelles showed that cross-linking of the PI corona can significantly increase the ceramic yields of the PFS block and shape retention by preventing the loss of potentially volatile PFS-derived fragmentation products.[55] Additionally, an

TABLE 2. Summary of the Dimensions of the Ceramic Arrays and the Size of the Iron Nanoparticles Produced from the Pyrolysis of PS, PFEMS, and Cylinder-Forming PS-*b*-PFEMS Block Copolymers

material	pyrolysis conditions[a]	$D_{c\text{-}c}$ (nm)[b]	d_{cyl} (nm)[c]	Fe NP size (nm) (SD)[d]
PS, bulk	1 °C/min to 600 °C			0
PFEMS, bulk	1 °C/min to 600 °C			~17.0 (3.7), 146 (31)
PS-*b*-PFEMS(0.36), bulk	1 °C/min to 600 °C	41.0	22.0	<1[e]
PS-*b*-PFEMS(0.36), bulk	15 °C/min to 600 °C	40.2	27.1	48.5 (12.1)
PS-*b*-PFEMS(0.25), thin film	1 °C/min to 600 °C	26.0	18.5	<1[e]
PS-*b*-PFEMS(0.25), thin film	UV cross-link then 1 °C/min to 600 °C	24.7	20.5	6.5 (0.7)

[a]To ensure complete ceramic conversion, the pyrolysis included a 5 h isothermal treatment at 600 °C following the heat ramp. [b]Determined from average value for >20 periods in an SEM image or for films, from SFM 2D Fourier transform. [c]Determined from average value for >30 cylinders. [d]Determined from average value for >30 nanoparticles. [e]On the basis of the lack of particles as determined by SEM and MFM, we assume the particle size to be less than 1 nm.[41,47,51,59,60]

interesting morphology was observed in the pyrolysis samples of UV cross-linked films where a Fe nanoparticle located on the top surface center of each ceramic cylinder (see Figure 4D). Presumably, the cross-linked PS matrix prevents the formation of NPs around the ceramic cylinders by eliminating the loss of potentially volatile PFS-derived fragmentation products. In contrast, at the unprotected top surface of the cylinder, the rapid loss of the fragments led to the Fe atom aggregation and exposure of the resulting Fe nanoparticles.[56]

MFM was used to investigate the magnetism of this cylinder-centered particle. Figure 4B shows the MFM image of semi-ordered arrays of magnetic ceramic domains showing cylinder-centered Fe nanoparticles. The detected magnetization of each particle increased with particle size, which is consistent with superparamagnetic, single-domain structures (diameter $<$10 nm).[57] Moreover, as a part of the particles is embedded in the ceramic post, the shape of the Fe particles is not clear. The magnetic shape anisotropy may also contribute to the observed magnetization.[57,58] Moreover, according to a 2D Fourier transform estimate of the periodicity, the ceramic lattice has been directly inherited from the diblock copolymer precursor film. In this case, d_{cyl} and $D_{c\text{-}c}$ were 20.5 and 24.7 nm, respectively. The average size of the ceramic cylinder-centered Fe nanoparticle is 6.5 nm. All nanoparticle sizes are summarized in Table 2.

Surface oxidation of the films was indicated in TGA studies of PS-*b*-PFEMS (Figure 1). To characterize the oxidation state of the surface of the ceramic films, we investigated the pyrolyzed PS-*b*-PFEMS(0.25) films (without and with UV cross-linking) using X-ray photoelectron spectroscopy (XPS). It has been previously shown that the Fe($2p_{1/2}$) and Fe($2p_{3/2}$) signals for PFS homopolymers are at 721.5 and 708.8 eV, respectively.[61] The iron XPS spectrum of the pyrolyzed thin film of PS-*b*-PFEMS(0.25) exhibits a set of split peaks at binding energies centered at ~725.9 and ~711.6 eV. A comparable spectrum was found for the UV cross-linked and pyrolyzed sample. Interestingly, Häussler *et al.*[62] have found a very similar XPS spectrum for pyrolyzed hyperbranched poly(ferrocenylene)s (*hb*-PFcs) with cross-linkable vinylsilane spacer units, and they have identified Fe_2O_3 as a species present at the ceramic surface.[63–65] Given the similarity between the XPS spectra of pyrolyzed PS-*b*-PFEMS(0.25) thin films with and without UV cross-linking and those of *hb*-PFcs, we reinforce our conclusions that the low pyrolysis heating rate (1 °C/min) favors the increased cross-linking of the ceramic matrix. As expected, cross-linking the PS domains by exposure to UV light therefore does not affect the surface composition of the resulting ceramics but rather improves the areal yield and shape retention during pyrolysis. This effect could be responsible for the formation of the well-defined, magnetic cylinder-centered iron nanoparticles observed by SFM, MFM, and SEM.

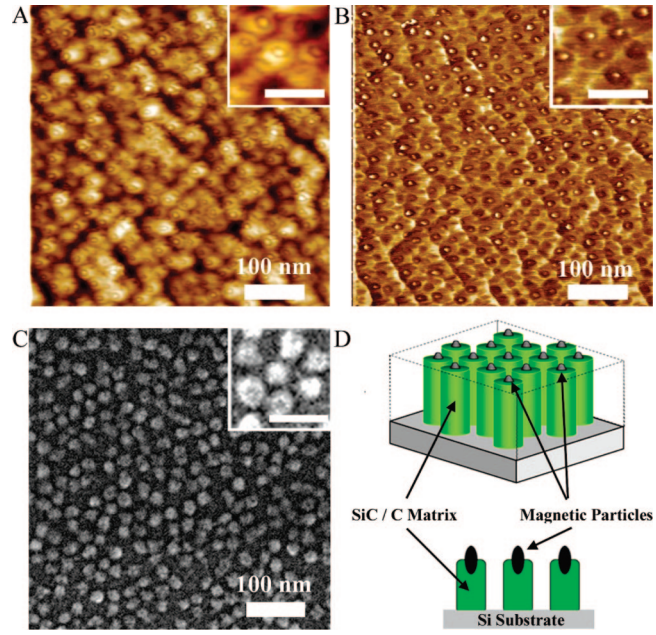

Figure 4. Height-mode scanning force (A), phase-mode magnetic force (B), and scanning electron (C) microscopy images of pyrolyzed, UV cross-linked PS-*b*-PFEMS(0.25) (1 °C/min to 600 °C for 5 h) (inset scale bars = 50 nm). (D) Depiction of the proposed structure resulting from the pyrolysis of UV cross-linked PS-*b*-PFEMS(0.25).

CONCLUSION

Detailed studies on the pyrolysis of cylinder-forming PS-*b*-PFEMS have confirmed that these materials are useful for the generation of semi-ordered arrays of iron- and silicon-containing ceramics. The ceramic mass yields are very predictable, and the nanostructuring of the self-assembled block copolymer controls the aggregation of iron nanoparticles. Due to the well-defined and nanometer-scaled dimensions of the preceramic PFEMS domains, there is limited lateral diffusion of free Fe atoms during the pyrolysis of PS-*b*-PFEMS thin films, and this gives rise to a monodisperse size distribution of the nanoparticles. The presence of a spatial diffusion barrier between the nanoscaled ceramics further prevents the aggregation of the monodisperse iron nanoparticles and hinders the formation of a significant population of larger particles, as observed for the case of PFS homopolymers.[45,48] When thin films of cylinder-forming block copolymers were pyrolyzed directly, low areal yields for the ceramics were observed. When the precursor film was stabilized through UV cross-linking of polystyrene, the areal yield of the inherited nanoceramics increased dramatically, leading to arrays of hexagonally packed cylinders with centered magnetic nanoparticles.

Our current efforts lie in the detailed, quantitative characterization of the magnetism generated using these thin-film processing techniques. This novel conceptual approach of producing nanostructured magnetic ceramics using a functional metal-containing block copolymer thin film as both a nanometer-scaled

template and an efficient preceramic material offers a promising pathway for the generation of high feature density technologies. With this in mind, we are currently targeting the development of analogous approaches to the patterning of nanostructured magnetic films based on hard magnetic materials such as FePt.

EXPERIMENTAL SECTION

Synthesis of Poly(ferrocenylethylmethylsilane) Homopolymer and Polystyrene-*block*-poly(ferrocenylethylmethylsilane) (PS-*b*-PFEMS) Diblock Copolymers and Casting of Bulk Samples. Complete synthetic details concerning the synthesis of the PFEMS and PS-*b*-PFEMS materials used in this study have been published elsewhere.[37] The casting of PS, PFEMS, and PS-*b*-PFEMS materials was repeated as previously described.[37]

Thin-Film Preparation and Annealing. PS-*b*-PFEMS films were prepared and annealed by solvent evaporation according to literature procedures.[53]

Pyrolysis of Bulk and Thin Films. PS-*b*-PFEMS films were pyrolyzed in a three-zone Thermacraft Inc. tube furnace. The films were placed in a quartz boat inside a quartz tube in the furnace, which was then purged with prepurified N_2 atmosphere for 30 min (1 L/min) prior to lowering the flow to *ca.* 50 mL/min for pyrolysis. The temperature of the tube furnace was increased at a rate of 1 °C/min to 600 °C.

SEM Analysis of Products from TGA Pyrolysis. Scanning electron microscopy (SEM) images were obtained using a Hitachi S-5200 electron microscope with an accelerating voltage of 1–15 kV. Approximately 0.2 mL of methanol was added to the sample pan (for the TA Instruments Q500) that was used for TGA analysis of PFEMS and PS-*b*-PFEMS(0.25). This was then placed in a small glass vial and sonicated for 15 min, after which one drop was pipetted onto a Formvar-coated TEM grid used as a support. Excess methanol was removed with filter paper, and the grid was allowed to dry at ambient conditions for 1 h. The grid was then mounted in the Hitachi scanning electron microscope for electron microscopy.

UV Polystyrene Cross-Linking of Thin Films. PS-*b*-PFEMS films were placed in a quartz Schlenk tube and evacuated (10^{-3} mm Hg), followed by exposure to UV light using a UVP Sterilaire lamp, model xx-15S (115 V, 60 Hz, 0.68 A), for 30 min.

Scanning Force Microscopy. Scanning force microscopy (SFM), operated in tapping mode, was performed on a Multimedia Nanoscope IIIa SFM (Digital Instruments/Veeco-Metrology Group). The SFM tips had resonant frequencies close to 170 kHz. The samples were mounted on steel sample pucks and imaged in air using an E-scanner (nominal maximum scan size of 13.5 μm^2). Image analysis was performed using the Digital Instruments Nanoscope software. All SFM/MFM data sets were collected as 512 $\times$ 512 pixel data sets with a scan rate of 1–1.5 Hz. Magnetic force microscopy (MFM) was performed following probe magnetization on the Multimode magnet holder. MFM images were acquired in lift mode (lift height = 5 nm), using tapping-mode SFM data for the same area to ensure a constant scan height above the sample. SFM phase images were also obtained for the same area to ensure that the MFM images were the result of magnetic forces and not physical surface interactions.

X-ray Photoelectron Spectroscopy. The surface of selected samples was investigated by X-ray photoelectron spectroscopy.[66] The obtained spectra, corrected for a carbon 1s binding energy of 284.5 eV, were compared with those of blank Si substrates to ensure that signals were mainly from our samples.

Acknowledgment. I.M. expresses his gratitude for the support of a Marie Curie Chair from the European Union and a Royal Society Wolfson Research Merit Award at Bristol. T.P.R. acknowledges funding from the U.S. Department of Energy, DEF0296ER45612. We are grateful to Chantal Paquet and Georgetta Masson for ellipsometry and TGA measurements, respectively. We also acknowledge the Ontario Government for OGSST and OGS Fellowships for D.A.R.

Supporting Information Available: AFM height image of a pyrolyzed cylinder-forming PS-*b*-PFEMS thin film that underwent a longer solvent annealing and a 30-min UV cross-linking before being pyrolyzed at 600 °C for 36 h. This material is available free of charge *via* the Internet at http://pubs.acs.org.

REFERENCES AND NOTES

1. Masuda, H.; Fukuda, K. Ordered Metal Nanohole Arrays Made by a Two-Step Replication of Honeycomb Structures of Anodic Alumina. *Science* **1995**, *268*, 1466–1468.
2. Gupta, R.; McClelland, J. J.; Jabbour, Z. J.; Celotta, R. J. Nanofabrication of a Two-Dimensional Array Using Laser-Focused Atomic Deposition. *Appl. Phys. Lett.* **1995**, *67*, 1378–1380.
3. Wendel, M.; Kuhn, S.; Lorenz, H.; Kotthaus, J. P.; Holland, M. Nanolithography with an Atomic Force Microscope for Integrated Fabrication of Quantum Electronic Devices. *Appl. Phys. Lett.* **1994**, *65*, 1775–1777.
4. Alexandridis, P.; Lindman, B. *Amphiphilic Block Copolymers: Self-Assembly and Applications*; Elsevier: Amsterdam, 2000.
5. Hamley, I. W. Nanotechnology with Soft Materials. *Angew. Chem., Int. Ed.* **2003**, *42*, 1692–1712.
6. Hawker, C. J.; Russell, T. P. Block Copolymer Lithography: Merging "Bottom-Up" with "Top-Down" Processes. *MRS Bull.* **2005**, *30*, 952–966.
7. Li, M. Q.; Ober, C. K. Block Copolymer Patterns and Templates. *Mater. Today* **2006**, *9*, 30–39.
8. Cheng, J. Y.; Ross, C. A.; Smith, H. I.; Thomas, E. L. Templated Self-Assembly of Block Copolymers: Top-Down Helps Bottom-Up. *Adv. Mater.* **2006**, *18*, 2505–2521.
9. Park, M.; Harrison, C.; Chaikin, P. M.; Register, R. A.; Adamson, D. H. Block Copolymer Lithography: Periodic Arrays of $\sim 10^{11}$ Holes in 1 Square Centimeter. *Science* **1997**, *276*, 1401–1404.
10. Yang, P.; Deng, T.; Zhao, D.; Feng, P.; Pine, D.; Chmelka, B. F.; Whitesides, G. M.; Stucky, G. D. Hierarchically Ordered Oxides. *Science* **1998**, *282*, 2244–2246.
11. Thurn-Albrecht, T.; Schotter, J.; Kästle, G. A.; Emley, N.; Shibauchi, T.; Krusin-Elbaum, L.; Guarin, K.; Black, C. T.; Tuominen, M. T.; Russell, T. P. Ultrahigh-Density Nanowire Arrays Grown in Self-Assembled Diblock Copolymer Templates. *Science* **2000**, *290*, 2126–2129.
12. Cheng, J. Y.; Ross, C. A.; Chan, V. Z.-H.; Thomas, E. L.; Lammertink, R. G. H.; Vancso, G. J. Formation of a Cobalt Magnetic Dot Array via Block Copolymer Lithography. *Adv. Mater.* **2001**, *13*, 1174–1178.
13. Naito, K.; Heida, H.; Sakurai, M.; Kamata, Y.; Asakawa, K. 2.5-Inch Disk Patterned Media Prepared by an Artificially Assisted Self-Assembling Method. *IEEE Trans. Magn.* **2002**, *38*, 1949–1951.
14. Garcia, C.; Zhang, Y.; DiSalvo, F.; Wiesner, U. Mesoporous Aluminosilicate Materials with Superparamagnetic γ-Fe_2O_3 Particles Embedded in the Walls. *Angew. Chem., Int. Ed.* **2003**, *42*, 1526–1530.
15. Rzayev, J.; Hillmyer, M. A. Nanoporous Polystyrene Containing Hydrophilic Pores from an ABC Triblock Copolymer Precursor. *Macromolecules* **2005**, *38*, 3–5.
16. Benkoski, J. J.; Bowles, S. E.; Korth, B. D.; Jones, R. L.; Douglas, J. F.; Karim, A.; Pyun, S. Y. Field Induced Formation of Mesoscopic Polymer Chains from Functional Ferromagnetic Colloids. *J. Am. Chem. Soc.* **2007**, *129*, 6291–6297.
17. Malenfant, P. R. L.; Wan, J.; Taylor, S. T.; Manoharan, M. Self-Assembly of an Organic-Inorganic Block Copolymer for Nano-Ordered Ceramics. *Nat. Nanotechnol.* **2007**, *2*, 43–46.

18. Kowalewski, T.; Tsarevsky, N. V.; Matyjaszewski, K. Nanostructured Carbon Arrays from Block Copolymers of Polyacrylonitrile. *J. Am. Chem. Soc.* **2002**, *124*, 10632–10633.
19. For a brief communication on some of this work, see: Temple, K.; Kulbaba, K.; Power-Billard, K. N.; Manners, I.; Leach, K. A.; Xu, T.; Russell, T. P.; Hawker, C. J. Spontaneous Vertical Ordering and Pyrolytic Formation of Nanoscopic Ceramic Patterns from Poly(styrene-*b*-ferrocenylsilane). *Adv. Mater.* **2003**, *15*, 297–300.
20. Krausch, G.; Magerle, R. Nanostructured Thin Films via Self-Assembly of Block Copolymers. *Adv. Mater.* **2002**, *14*, 1579–1583.
21. Matsen, M. W.; Bates, F. S. Unifying Weak- and Strong-Segregation Block Copolymer Theories. *Macromolecules* **1996**, *29*, 1091–1098.
22. Archer, R. D. *Inorganic and Organometallic Polymers*; Wiley VCH: Weinheim, 2001.
23. Whittell, G. R.; Manners, I. Metallopolymers: New Multifunctional Materials. *Adv. Mater.* **2007**, *19*, 3439–3468.
24. Kulbaba, K.; Manners, I. Polyferrocenylsilanes: Metal-Containing Polymers for Materials Science, Self-Assembly and Nanostructure Applications. *Macromol. Rapid Commun.* **2001**, *22*, 711–724.
25. Manners, I. Polymer Science with Transition Metals and Main Group Elements: Towards Functional, Supramolecular Inorganic Polymeric Materials. *J. Polym. Sci., Part A: Polym. Chem.* **2002**, *40*, 179–191.
26. Rider, D. A.; Manners, I. Synthesis, Self-Assembly, and Applications of Polyferrocenylsilane Block Copolymers. *Polym. Rev.* **2007**, *47*, 165–195.
27. Bellas, V.; Rehahn, M. Polyferrocenylsilane-Based Polymer Systems. *Angew. Chem., Int. Ed.* **2007**, *46*, 5082–5104.
28. Korczagin, I.; Lammertink, R. G. H.; Hempenius, M. A.; Golze, S.; Vancso, G. J. Surface Nano- and Microstructuring with Organometallic Polymers. *Adv. Polym. Sci.* **2006**, *200*, 91–117.
29. Ni, Y.; Rulkens, R.; Manners, I. Transition Metal-Based Polymers with Controlled Architectures: Well-Defined Poly(ferrocenylsilane) Homopolymers and Multiblock Copolymers via the Living Anionic Ring-Opening Polymerization of Silicon-Bridged [1]Ferrocenophanes. *J. Am. Chem. Soc.* **1996**, *118*, 4102–4114.
30. Tanabe, M.; Vandermeulen, G. W. M.; Chan, W. Y.; Cyr, P. W.; Vanderark, L.; Rider, D. A.; Manners, I. Photocontrolled Living Polymerizations. *Nat. Mater.* **2006**, *5*, 467–470.
31. Massey, J. A.; Power, K. N.; Winnik, M. A.; Manners, I. Organometallic Nanostructures: Self-Assembly of Poly(ferrocene) Block Copolymers. *Adv. Mater.* **1998**, *10*, 1559–1562.
32. Lammertink, R. G. H.; Hempenius, M. A.; Thomas, E. L.; Vancso, G. J. Periodic Organic-Organometallic Microdomain Structures in Poly(styrene-*block*-ferrocenyldimethylsilane) Copolymers and Blends with Corresponding Homopolymers. *J. Polym. Sci., Part B: Polym. Phys.* **1999**, *37*, 1009–1021.
33. Li, W.; Sheller, N.; Foster, M. D.; Balaishis, D.; Manners, I.; Annis, I.; Lin, J. S. Morphology and Ordering Behavior of a Poly(styrene) -*b*-Poly(ferrocenyldimethylsilane) Diblock Copolymer. *Polymer* **2000**, *41*, 719–724.
34. Eitouni, H. B.; Balsara, N. P.; Hahn, H.; Pople, J. A.; Hempenius, M. A. Thermodynamic Interactions in Organometallic Block Copolymers: Poly(styrene-*block*-ferrocenyldimethylsilane). *Macromolecules* **2002**, *35*, 7765–7772.
35. Kloninger, C.; Rehahn, M. 1,1-Dimethylsilacyclobutane-Mediated Living Anionic Block Copolymerization of [1]Dimethylsilaferrocenophane and Methyl Methacrylate. *Macromolecules* **2004**, *37*, 1720–1727.
36. Datta, U.; Rehahn, M. Synthesis and Self-Assembly of Styrene-[1]Dimethylsilaferrocenophane-Methyl Methacrylate Pentablock Copolymers. *Macromol. Rapid Commun.* **2004**, *25*, 1615–1622.
37. Rider, D. A.; Cavicchi, K. A.; Power-Billard, K. N.; Russell, T. P.; Manners, I. Diblock Copolymers with Amorphous Atactic Polyferrocenylsilane Blocks: Synthesis, Characterization, and Self-Assembly of Polystyrene-*block*-poly(ferrocenylethylmethylsilane) in the Bulk State. *Macromolecules* **2005**, *38*, 6931–6938.
38. Eitouni, H. B.; Balsara, N. P. Electrochemically Controlled Self-Assembly of an Organometallic Block Copolymer. *J. Am. Chem. Soc.* **2006**, *128*, 16248–16252.
39. Manners, I. Poly(ferrocenylsilanes): Novel Organometallic Plastics. *Chem. Commun.* **1999**, 857–865.
40. Eitouni, H. B.; Balsara, N. P. Effect of Chemical Oxidation on the Self-Assembly of Organometallic Block Copolymers. *J. Am. Chem. Soc.* **2004**, *126*, 7446–7447.
41. Lastella, S.; Jung, Y. J.; Yang, H.; Vajtai, R.; Ajayan, P. M.; Ryu, C. Y.; Rider, D. A.; Manners, I. Density Control of Single-Walled Carbon Nanotubes Using Patterned Iron Nanoparticle Catalysts Derived from Phase-Separated Thin Films of a Polyferrocene Block Copolymer. *J. Mater. Chem.* **2004**, *14*, 1791–1794.
42. Hinderling, C.; Keles, Y.; Stoeckli, T.; Knapp, H. F.; De Los Arcos, T.; Oelhafen, P.; Korczagin, I.; Hempenius, M. A.; Vancso, G. J.; Pugin, R. Organometallic Block Copolymers as Catalyst Precursors for Templated Carbon Nanotube Growth. *Adv. Mater.* **2004**, *16*, 876–879.
43. For the formation of SiC/C ceramics containing Fe and Fe_xO_y nanoparticles from the pyrolysis of PFS homopolymers, see: Petersen, R.; Foucher, D. A.; Tang, B.-Z.; Lough, A.; Raju, N. P.; Greedan, J. E.; Manners, I. Pyrolysis of Poly(ferrocenylsilanes): Synthesis and Characterization of Ferromagnetic Transition-Metal-Containing Ceramics and Molecular Depolymerization Products. *Chem. Mater.* **1995**, *7*, 2045–2053.
44. MacLachlan, M. J.; Ginzburg, M.; Coombs, N.; Coyle, T. W.; Raju, N. P.; Greedan, J. E.; Ozin, G. A.; Manners, I. Shaped Ceramics with Tunable Magnetic Properties from Metal-Containing Polymers. *Science* **2000**, *287*, 1460–1463.
45. Kulbaba, K.; Cheng, A.; Bartole, A.; Greenberg, S.; Resendes, R.; Coombs, N.; Safa-Sefat, A.; Greedan, J. E.; Stöver, H. D. H.; Ozin, G. A.; Manners, I. Polyferrocenylsilane Microspheres: Synthesis, Mechanism of Formation, Size and Charge Tunability, Electrostatic Self- Assembly, and Pyrolysis to Spherical Magnetic Ceramic Particles. *J. Am. Chem. Soc.* **2002**, *124*, 12522–12534.
46. Sun, Q.; Lam, J. W. Y.; Xu, K.; Xu, H.; Cha, J. A. K.; Wong, P. C. L.; Wen, G.; Zhang, X.; Jing, X.; Wang, F. Nanocluster-Containing Mesoporous Magnetoceramics from Hyperbranched Organometallic Polymer Precursors. *Chem. Mater.* **2000**, *12*, 2617–2624.
47. Lu, J. Q.; Kopley, T. E.; Moll, N.; Roitman, D.; Chamberlin, D.; Fu, Q.; Liu, J.; Russell, T. P.; Rider, D. A.; Manners, I.; Winnik, M. A. High-Quality Single-Walled Carbon Nanotubes with Small Diameter, Controlled Density, and Ordered Locations Using a Polyferrocenylsilane Block Copolymer Catalyst Precursor. *Chem. Mater.* **2005**, *17*, 2227–2231.
48. Ginzburg, M.; MacLachlan, M. J.; Yang, S. M.; Coombs, N.; Coyle, T. W.; Raju, N. P.; Greedan, J. E.; Herber, R. H.; Ozin, G. A.; Manners, I. Genesis of Nanostructured, Magnetically Tunable Ceramics from the Pyrolysis of Cross-Linked Polyferrocenylsilane Networks and Formation of Shaped Macroscopic Objects and Micron Scale Patterns by Micromolding Inside Silicon Wafers. *J. Am. Chem. Soc.* **2002**, *124*, 2625–2639.
49. In spite of the inert nitrogen atmosphere purge, the mass composition is observed to increase by ~2% during the heating from 415 to 600 °C. This effect is reproducible and is only observed in PS-*b*-PFEMS samples.
50. On the basis of carbon nanotube (CNT) growth studies, we assume that the iron nanoparticle diameter is similar to that of the CNTs and therefore <1 nm. Please see: Lastella, S.; Mallick, G.; Woo, R.; Karna, S. P.; Rider, D. A.; Manners, I.; Jung, Y. J.; Ryu, C. Y.; Ajayan, P. M. Influences of Organometallic Polymer-Derived Catalyst Dispersion on SWNT Growth. *J. Polym. Sci. B: Polym. Phys.* **2007**, *45*, 758–765.

51. Lastella, S.; Mallick, G.; Woo, R.; Karna, S. P.; Rider, D. A.; Manners, I.; Jung, Y. J.; Ryu, C. Y.; Ajayan, P. M. Parallel Arrays of Individually Addressable Single-Walled Carbon Nanotube Field-Effect Transistors. *J. Appl. Phys.* **2006**, *99*, 024302.
52. Kim, S. H.; Misner, M.; Xu, T.; Kimura, M.; Russell, T. P. Highly Oriented and Ordered Arrays from Block Copolymers via Solvent Evaporation. *Adv. Mater.* **2004**, *16*, 226–231.
53. Rider, D. A.; Cavicchi, K. A.; Vanderark, L.; Russell, T. P.; Manners, I. Orientationally Controlled Nanoporous Cylindrical Domains in Polystyrene-*b*-poly(ferrocenylethylmethylsilane) Block Copolymer Films. *Macromolecules* **2007**, *40*, 3790–3796.
54. Polystyrene is known to undergo both chain scission and cross-linking pathways when exposed to UV light. In our case, the dominant pathway was determined to be the latter, as the UV-exposed PS-*b*-PFEMS films were found to be stable to dissolution in various solvents. See: Rånby, B.; Rabek, J. F. *Photodegradation, Photo-oxidation and Photostabilization of Polymers*; Wiley: New York, NY, 1975.
55. Wang, X.; Liu, K.; Arsenault, A. C.; Rider, D. A.; Ozin, G. A.; Winnik, M. A.; Manners, I. Shell-Cross-Linked Cylindrical Polyisoprene-*b*-Polyferrocenylsilane (PI-*b*-PFS) Block Copolymer Micelles: One-Dimensional (1D) Organometallic Nanocylinders. *J. Am. Chem. Soc.* **2007**, *129*, 5630–5639.
56. Liu, K.; Clendenning, S. B.; Friebe, L.; Chan, W. Y.; Zhu, X. B.; Freeman, M. R.; Yang, G. C.; Yip, C. M.; Grozea, D.; Lu, Z.-H. Pyrolysis of Highly Metallized Polymers: Ceramic Thin Films Containing Magnetic CoFe Alloy Nanoparticles from a Polyferrocenylsilane with Pendant Cobalt Clusters. *Chem. Mater.* **2006**, *18*, 2591–2601.
57. Leslie-Pelecky, D. L.; Rieke, R. D. Magnetic Properties of Nanostructured Materials. *Chem. Mater.* **1996**, *8*, 1770–1783.
58. Lu, A.-H.; Salabas, E. L.; Schüth, F. Magnetic Nanoparticles: Synthesis, Protection, Functionalization, and Application. *Angew. Chem., Int. Ed.* **2007**, *46*, 1222–1244.
59. Lu, J. Q.; Rider, D. A.; Onyegam, E.; Wang, H.; Winnik, M. A.; Manners, I.; Cheng, Q.; Fu, Q.; Liu, J. Carbon Nanotubes with Small and Tunable Diameters from Poly(ferrocenylsilane)-*block*-Polysiloxane Diblock Copolymers. *Langmuir* **2006**, *22*, 5174–5179.
60. Lastella, S.; Mallick, G.; Woo, R.; Karna, S. P.; Rider, D. A.; Manners, I.; Jung, Y. J.; Ryu, C. Y.; Ajayan, P. M. Influences of Organometallic Polymer-Derived Catalyst Dispersion on SWNT Growth. *J. Polym. Sci. B: Polym. Phys.* **2007**, *45*, 758–765.
61. Lammertink, R. G. H.; Hempenius, M. A.; Chan, V. Z.-H.; Thomas, E. L.; Vancso, G. J. Poly(ferrocenyldimethylsilanes) for Reactive Ion Etch Barrier Applications. *Chem. Mater.* **2001**, *13*, 429–434.
62. Häussler, M.; Sun, Q.; Xu, K.; Lam, J. W. Y.; Dong, H.; Tang, B.-Z. Hyperbranched Poly(ferrocenylene)s Containing Groups 14 and 15 Elements: Syntheses, Optical and Thermal Properties, and Pyrolytic Transformations into Nanostructured Magnetoceramics. *J. Inorg. Organomet. Polym. Mater.* **2005**, *15*, 67–81.
63. The signals for Fe_2O_3 are at 725.3 and 711.4 eV. It is possible that FeOOH is present as well, since its XPS binding energy (711.7 eV) is near this signal.
64. Moulder, J. F.; Stickle, W. F.; Sobol, P. E.; Bomden, K. D. *Handbook of X-Ray Photoelectron Spectroscopy: a Reference Book of Standard Spectra for Identification and Interpretation of XPS Data*; Physical Electronics Division, Perkin-Elmer Corp.: Eden Prairie, MN, 1992.
65. Fradley, C. S. In *Electron Spectroscopy*; Shirley, D. A., Ed.; North Holland: Amsterdam, 1972.
66. Briggs, D.; Seah, M. P. *Practical Surface Analysis: by Auger and X-Ray Photoelectron Spectroscopy*; Wiley: Chichester, UK, 1983.